

## Effects of positron spin polarization on orthopositronium and parapositronium formation in a magnetic field

Y. Nagashima and T. Hyodo

*Institute of Physics, College of Arts and Sciences, University of Tokyo 3-8-1 Komaba, Meguro-ku, Tokyo 153, Japan*

(Received 14 August 1989)

Formation of positronium in porous silica glass by spin-polarized positrons in the presence of a magnetic field is investigated using a one-dimensional angular-correlation apparatus. Asymmetric field dependences of the formation probabilities of both perturbed orthopositronium and perturbed parapositronium are analyzed in a wide range of the field. The feasibility of the application of the angular-correlation method to positron spin polarimetry is discussed.

### I. INTRODUCTION

Since parity is not conserved in the weak interaction, the positrons emitted in  $\beta$  decay are spin polarized along their momenta. One of the most sensitive methods to measure the polarization of the positrons is to use positronium (Ps) formation in the presence of an applied magnetic field.<sup>1,2</sup> It is well known that Ps has two ground states.<sup>2-4</sup> Para-Ps (singlet,  $m=0$ ) self-annihilates into  $2\gamma$ ; ortho-Ps (triplet,  $m=0, \pm 1$ ) into  $3\gamma$ . In a static magnetic field, the para-Ps state and the  $m=0$  substate of ortho-Ps are no longer the eigenstates but their mixtures (linear combinations) become the new ones, while the  $m=\pm 1$  substates are not affected. Both the new eigenstates can annihilate into  $2\gamma$  or  $3\gamma$ . (We shall refer to the perturbed  $m=0$  ortho-Ps as ortho-like-Ps and the perturbed para-Ps as para-like-Ps.) When Ps is formed by polarized positrons, the formation of para-like-Ps or ortho-like-Ps is favored depending on whether the positrons are polarized parallel or opposite to the magnetic field. Page and Heinberg<sup>1</sup> noticed that this asymmetry can be used to construct a positron polarimeter if one can distinguish the two Ps states from each other. These authors produced Ps in a high-pressure Ar gas and measured the peak counts of the angular correlation of annihilation radiation (ACAR) curve. In this method the Ps states were distinguished through their average momenta which are different because long-lived ortho-like-Ps is more thermalized than short-lived para-like-Ps.

Direct use of the lifetime difference to distinguish the Ps states was suggested by Telegdi<sup>5</sup> and Lundby<sup>6</sup> and carried out by Dick *et al.*<sup>7</sup> and Bisi *et al.*<sup>8</sup> This method has been improved by Rich and co-workers and used in the study of the weak interaction<sup>9,10</sup> and other applications.<sup>11</sup>

Improvement of the ACAR-based polarimeter, on the other hand, has never been attempted since the first successful measurements by Page and Heinberg.<sup>1</sup> In this paper we report measurements which show that the capability of the ACAR based polarimeter can be expanded by an appropriate choice of a Ps formation medium. We have measured magnetic field dependence of the Ps formation probability in porous silica glass in a wide range of magnetic fields and compared the results with theory.

The present method provides a convenient way to measure the polarization of the ensemble of positrons which impinge on the sample in an actual ACAR apparatus.

### II. THEORETICAL BACKGROUND

The fractions of ortho-like-Ps and para-like-Ps formed from polarized positrons in the magnetic field  $\mathbf{B}$  are

$$F_{o'} = \frac{1}{8(1+y^2)} [(1+y)^2(1-P) + (1-y)^2(1+P)], \quad (1)$$

$$F_{p'} = \frac{1}{8(1+y^2)} [(1-y)^2(1-P) + (1+y)^2(1+P)], \quad (2)$$

respectively, where  $y$  is given by  $y = x / [(1+x^2)^{1/2} + 1]$  with  $x = 4\mu B / \hbar\omega_0$ , and  $P$  is the polarization of the positrons along  $\mathbf{B}$  at the instant of the Ps formation.<sup>8</sup>  $\mu$  is the magnetic moment of the electron and  $\hbar\omega_0$  is the hyperfine structure splitting between ortho-Ps and para-Ps. The self-annihilation rates of ortho-like-Ps and para-like-Ps are  $\gamma_{o'} = (\gamma_o + y^2\gamma_p) / (1+y^2)$  and  $\gamma_{p'} = (y^2\gamma_o + \gamma_p) / (1+y^2)$ , where  $\gamma_o$  and  $\gamma_p$  are the self-annihilation rates of ortho-Ps and para-Ps, respectively. For Ps in a vacuum,  $\gamma_o = 7.05 \times 10^6 \text{ s}^{-1}$ ,  $\gamma_p = 7.99 \times 10^9 \text{ s}^{-1}$ , and  $\hbar\omega_0 = 8.4 \times 10^{-4} \text{ eV}$ ,<sup>2,3</sup> while these values are different in materials.<sup>4,8</sup> Since both ortho-like-Ps and para-like-Ps can self-annihilate into  $2\gamma$ , it is possible to get information on  $F_{o'}$  and  $F_{p'}$  and hence on  $P$  with the ACAR method, which is exclusively sensitive to the  $2\gamma$  events. The components in one-dimensional (1D) ACAR resulting from the self-annihilation of ortho-like-Ps and para-like-Ps are

$$N_{o'}(p_z) \propto \frac{\gamma_p}{\Gamma_{o'}} \frac{y^2}{1+y^2} F_{o'} n_{o'}(p_z) = I_{o'} n_{o'}(p_z) \quad (3)$$

and

$$N_{p'}(p_z) \propto \frac{\gamma_p}{\Gamma_{p'}} \frac{1}{1+y^2} F_{p'} n_{p'}(p_z) = I_{p'} n_{p'}(p_z), \quad (4)$$

respectively, where  $n_{o'}(p_z)$  and  $n_{p'}(p_z)$  are the normalized ACAR curves for the respective components and  $p_z = mc\theta$ ,  $\theta$  being the departure from  $180^\circ$  of the annihilation

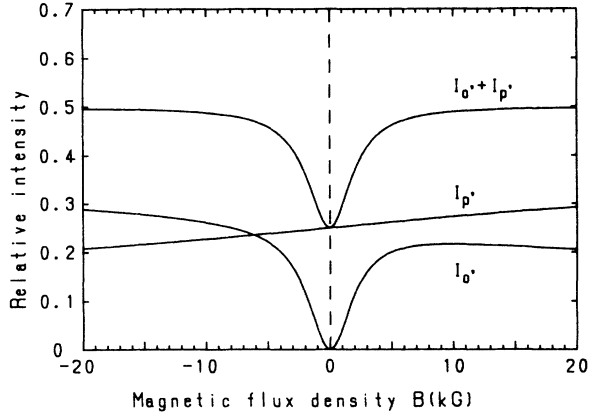


FIG. 1. Theoretical  $2\gamma$  annihilation intensities of ortho-like-Ps ( $I_o$ ) and para-like-Ps ( $I_p$ ) in a vacuum with  $P=0.35$  as functions of magnetic flux density. Total number of Ps atoms is normalized to 1.  $B > 0$  corresponds to the field pointing parallel to the average momentum of the positrons.

lation quanta.  $\Gamma_o$  and  $\Gamma_p$  indicate the total annihilation rates of the ortho-like-Ps and para-like-Ps, respectively, including all possible quenching rates. (Only for free Ps in a vacuum do  $\Gamma_o = \gamma_o$  and  $\Gamma_p = \gamma_p$  hold.) As Page and Heinberg<sup>1</sup> pointed out, the two states can be distinguished on an ACAR curve if Ps is formed in a substance in which the Ps thermalization time is much longer than the para-like-Ps lifetime. In their experiments using high-pressure Ar gas to produce and moderate Ps, however, they did not measure the partial profiles  $N_o(p_z)$  or  $N_p(p_z)$  but only measured the polarization effect on the peak (i.e.,  $p_z=0$ ) count rate of ACAR.

In the present experiment we attempt to separate  $N_o(p_z)$  from  $N_p(p_z)$  in ACAR in porous silica glass. Once they are separated, the intensities  $I_o$  and  $I_p$  are given by the areas defined as  $I_o = \int N_o(p_z) dp_z$ , etc. Figure 1 illustrates the theoretically expected intensities  $I_o$ ,  $I_p$ , and  $I_o + I_p$  for the case of  $P=0.35$  in a vacuum. Note that while  $I_o + I_p$  is almost symmetric around  $B=0$ ,  $I_o$  and  $I_p$  are not. The dip in  $I_o$  at  $B=0$  results from the inhibition of the  $2\gamma$  annihilation of ortho-Ps.

### III. EXPERIMENTAL PROCEDURE

We measured the momentum distribution of the  $\gamma$  rays from positrons annihilating in porous silica glass using the 1D-ACAR apparatus. The measurements were performed at room temperature. The momentum resolution of the apparatus was  $0.5 \times 10^{-3} mc$ . The dimensions of the porous glass sample were  $20 \times 15 \times 4 \text{ mm}^3$ . The mean diameter of the pore was about  $37 \text{ \AA}$  and the porosity was 40.2%. The sample was set in a vacuum-tight sample chamber which had a window of  $40 \text{ \mu m Be}$ . A positron source of 5-mCi  $^{22}\text{Na}$  was set just outside the Be window. The chamber was placed in a magnetic field up to  $\pm 16 \text{ kG}$ . The coincidence counts were accumulated with the field pointing parallel or antiparallel to the average momentum of the positrons impinging on the sample. The data for the opposite magnetic fields were taken by

reversing the field at each stop of the counter. A typical spectrum took a few weeks to accumulate.

### IV. RESULTS AND DATA ANALYSIS

Figure 2 illustrates the ACAR data taken for  $B=0 \sim +16.0 \text{ kG}$ , and in Fig. 3 the differences between the data for opposite field directions are shown.  $B > 0$  indicates the field pointing parallel to the average momentum of the incident positrons. The difference curves have a dip at  $p_z=0$  and bumps around  $p_z = \pm 1.2 \times 10^{-3} mc$ . This is quite unusual in comparison with the difference curves for usual condensed matters, which show a single peak at  $p_z=0$ .<sup>12-14</sup> However, a straightforward interpretation is possible if one takes into account the  $B$  dependence of  $I_o$  and  $I_p$  shown in Fig. 1, and that the thermalization of Ps in the pore is relatively slow. The Ps atoms are formed in the bulk<sup>15</sup> and then ejected into the pore region with kinetic energy determined by the negative

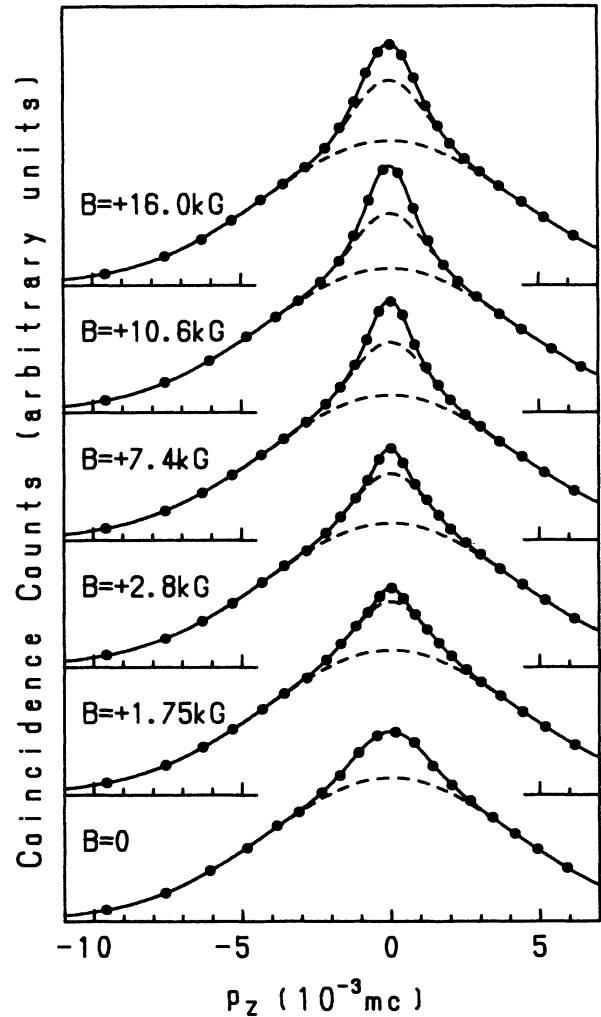


FIG. 2. ACAR data for  $B=0 \sim +16.0 \text{ kG}$ . The dashed curves show the decompositions into Gaussian components made by a nonlinear least-squares analysis. The data have been normalized to have the same broad component intensity.

work function of the pore surface for Ps.<sup>16</sup> They gradually lose energy as they hit the pore surface many times. Since ortho-like-Ps in the pore lives much longer than para-like-Ps, it loses more kinetic energy than para-like-Ps. Thus  $N_{o'}(p_z)$  is narrower than  $N_{p'}(p_z)$ .

The whole ACAR data in a magnetic field certainly show that there exist more than one component (Fig. 2). For a quantitative analysis, however, we must take into account that some of the Ps atoms annihilate in the bulk region before escaping into a pore. The ACAR curve for porous materials in a magnetic field, in general, consists of the components from the  $2\gamma$  branches of the following processes: (i) self-annihilation of ortho-like-Ps in the pore; (ii) self-annihilation of para-like-Ps in the pore; (iii) self-annihilation of ortho-like-Ps in the bulk; (iv) self-annihilation of para-like-Ps in the bulk; (v) pickoff annihilation of Ps; (vi) annihilation of non-Ps positrons. It is impossible to decompose the data into all of these components. We thus decomposed them into three Gaussian components, narrow, middle, and broad ones. The fitting

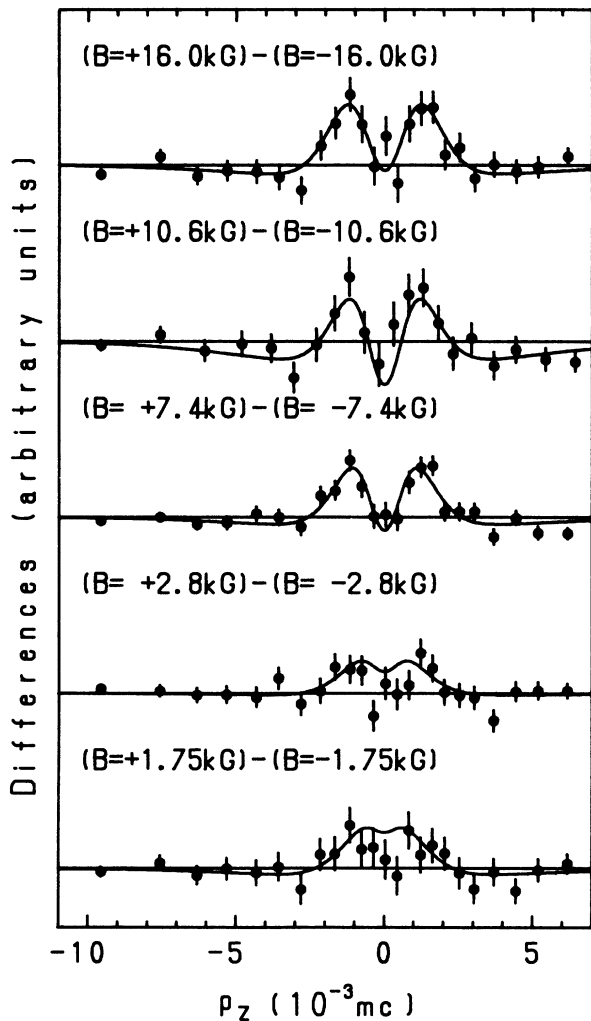


FIG. 3. Differences between the ACAR data for the fields in the opposite directions. The solid curves show the theoretical differences calculated with the optimized parameters.

procedure was as follows. First, constraint-free three-Gaussian fits were performed. The width of the broad component was found to be about the same for all the data. Then, the second fits were done with the width of the broad component fixed to the average value  $9.7 \times 10^{-3} mc$ . It was found that the width of the middle component was again almost constant for all the data. The average of the width was  $2.7 \times 10^{-3} mc$ . The final fits were performed with the widths of these two wider components fixed. Since the lifetime of Ps is independent of the polarity of  $\mathbf{B}$ , the fits to the ACAR curves for  $\pm B$  were made simultaneously with a constraint that the width of the narrow component should be the same.<sup>17</sup>

The obtained intensities of the narrow component,  $I_n$ , and of the middle component,  $I_m$ , relative to the intensities of the broad components are plotted in Fig. 4, while the width of the narrow component is plotted in Fig. 5, against the magnetic flux density. We interpret that the narrow component represents  $N_{o'}(p_z)$  because it is not observed when  $B=0$  and its width becomes broader at higher magnetic fields as shown in Fig. 5: Note that (a) ortho-Ps in zero field does not self-annihilate into  $2\gamma$  and (b) since the lifetime of ortho-like-Ps becomes shorter with increasing  $B$ ,  $N_{o'}(p_z)$  is expected to show less thermalized distribution.<sup>18,19</sup> The length of the error bars in Fig. 4 has been determined by diagonal terms of the error matrix given by the least-squares analysis. The larger errors at higher magnetic fields reflect the difficulty of separation of the two components because of the broadening of the narrow component. The field dependence of the width of  $N_{o'}(p_z)$  indicates that the Ps atoms are free in the pore in contradiction to the suggestion of the possibility of Ps bound on the pore surface by Kim and Buyers.<sup>15</sup> The fact that there was no narrow peak in the ACAR data for  $B=0$  also shows that the pores were evacuated enough to eliminate the oxygen-induced ortho-para conversion effect.<sup>20</sup> The middle component should represent (ii) + (iii) + (iv). There are two observations which support this assignment. (a) The momentum distribution of para-Ps in silica powders with an average free space diameter of  $57 \text{ \AA}$ , not much different from the pore diameter of the present glass, has a width of about  $3 \times 10^{-3} mc$ .<sup>18</sup> The para-Ps component observed in ordinary silica glass has a width of  $2.9 \times 10^{-3} mc$ .<sup>21</sup> The latter represents the zero-point motion of the Ps trapped in the disorder of amorphous silica. Finally the broad component should represent (v) + (vi). The width of this component is largely determined by the momentum distribution of the electrons bound in  $\text{SiO}_2$ .

The curves in Fig. 4 show the results of the nonlinear least-squares fit of the following functions to the experimental intensities of the narrow and middle components:

$$I_n(\mathbf{B}) = \frac{\gamma_e}{\Gamma_{o'}^{\text{bulk}}} I_{o'}^{\text{pore}}, \quad (5)$$

$$I_m(\mathbf{B}) = \frac{\gamma_e}{\Gamma_{p'}^{\text{bulk}}} I_{p'}^{\text{pore}} + (I_{o'}^{\text{bulk}} + I_{p'}^{\text{bulk}}). \quad (6)$$

Here,  $I_{o'}^{\text{pore}}$  and  $I_{p'}^{\text{pore}}$  represent the intensities of the ortho-like-Ps and para-like-Ps components in the pore, respectively. They are given by Eqs. (3) and (4) with  $\Gamma_{o'}$

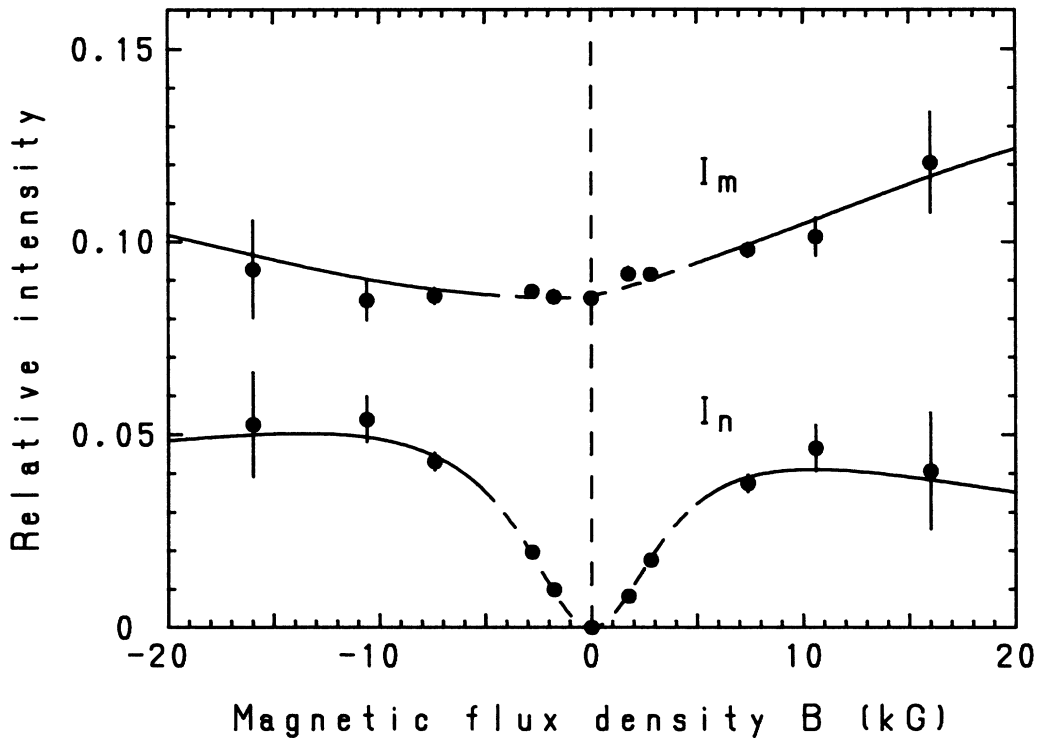


FIG. 4. Intensities of the middle component ( $I_m$ ) and the narrow component ( $I_n$ ) relative to the intensity of the broad component as functions of the magnetic flux density. Also shown are theoretical curves fitted for  $|B| \geq 7.4$  kG. The parts of the curves in the region  $-5 \text{ kG} \lesssim B \lesssim 5 \text{ kG}$  are shown by the dashed lines.

and  $\Gamma_p$ , including the pickoff rate in the pore. The coefficients of  $I_o^{\text{pore}}$  and  $I_p^{\text{pore}}$  represent the fractions of the Ps atoms which escape into the pore,  $\gamma_e$  being the escape rate.  $\Gamma_o^{\text{bulk}}$  and  $\Gamma_p^{\text{bulk}}$  are the total annihilation rates in the bulk plus  $\gamma_e$ . The pickoff rate in the bulk was determined to be  $(6.24 \pm 0.02) \times 10^8 \text{ s}^{-1}$  by a positron lifetime

measurement for the normal silica glass made from the same raw material as the present porous glass sample.  $I_o^{\text{bulk}}$  and  $I_p^{\text{bulk}}$  are the intensities of the ortho-like-Ps and para-like-Ps components in the bulk. We approximate these by Eqs. (3) and (4) with  $\Gamma_o$  and  $\Gamma_p$  replacing  $\Gamma_o^{\text{bulk}}$  and  $\Gamma_p^{\text{bulk}}$ , respectively. We assumed for the sake of simplicity that the self-annihilation rates and the hyperfine splitting of Ps in the bulk is the same as in a vacuum.

The free parameters in the fitting were the positron polarization  $P$ , the escape rate  $\gamma_e$ , the pickoff rate in the pore, and a common normalization factor which is not included in Eqs. (5) and (6). In order to determine the parameters except for  $P$ , we first fitted  $I_n(B) + I_n(-B)$  and  $I_m(B) + I_m(-B)$  to the sum of the experimental intensities for the fields of the same magnitude and opposite directions. Note that these sums are independent of  $P$ . The two sums were fitted simultaneously.<sup>17</sup> The escape rate and the pickoff rate in the pore were determined to be  $(9.7 \pm 1.1) \times 10^8$  and  $(1.7 \pm 0.2) \times 10^7 \text{ s}^{-1}$ , respectively. (The pickoff rate for thermalized Ps atoms measured in a sample cut from the same porous glass by the lifetime technique was  $3.1 \times 10^6 \text{ s}^{-1}$ , several times lower than the above value. This is probably because nonthermal Ps atoms not only hit the pore surface more frequently but also may have a closer encounter with the surface atoms.<sup>19</sup>) Then, with these polarization-independent parameters fixed, we fitted  $I_n(B)$  and  $I_m(B)$  to the corresponding experimental intensities for  $|B| \geq 7.4$  kG to obtain the polarization  $P$ .<sup>17</sup> The optimum value for  $P$  was  $0.34 \pm 0.06$ . We restricted the range of the field in the fitting because the effective energy spectrum of the posi-

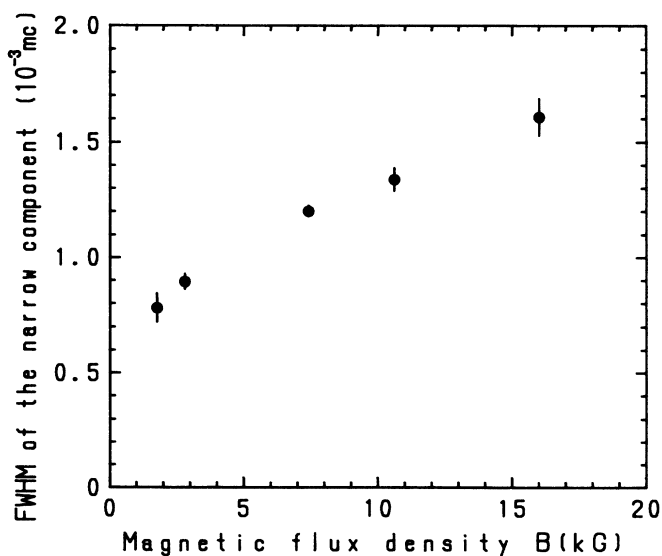


FIG. 5. Full width at half maximum of the narrow component plotted against the magnetic flux density. The effect of the experimental resolution has been corrected by quadratic deconvolution.

trons impinging on the sample, and hence the average polarization of the positrons depends on the field intensity. The stronger the magnetic field is, the more positrons with relatively large transverse momentum component spiral into the sample. We found that the partial count rate corresponding to the broad component increased with  $|B|$ , but became almost constant in the region  $|B| \geq 7.4$  kG, showing that almost all the forward positrons went into the sample in a high field. The averaged polarization in the weaker field was  $0.34 \pm 0.14$  in  $|B| = 2.8$  kG and  $0.7 \pm 0.3$  in  $|B| = 1.75$  kG. These values were obtained by analyzing the data for each field individually. The differences between the ACAR curves for the fields of the same magnitude and opposite directions calculated with thus determined parameters (i.e.,  $P = 0.34$  for  $|B| \geq 2.8$  kG and  $P = 0.7$  for  $|B| = 1.75$  kG) are shown by the solid curves in Fig. 3.

### V. DISCUSSIONS

The value of the polarization  $P$  obtained here represents that averaged over all the positrons actually forming Ps in the sample. It includes the effects of the scattering of the positrons by the backing of the source assembly, the absorption of the positrons by Ti cover of the source and the Be window of the chamber, the convergence of positrons by the magnetic field, and the depolarization during the thermalization. The precision of the obtained value of the effective polarization is 18%. This is apparently better than that of Page and Heinberg, but worse than that attained by the lifetime method (5%).<sup>9</sup> The precision is expected to be improved with a choice of a better Ps formation medium (i) which is dense enough to stop the  $\beta^+$  particles in a thin region necessary for a high resolution ACAR measurement, and (ii) in which bulk Ps component intensity is sufficiently low. Porous glass used in the present work has the quality (i) but not the quality (ii). On the contrary, high-pressure gases as were used by Page and Heinberg,<sup>1</sup> have the quality (ii) but not (i). A compressed very fine  $\text{SiO}_2$  or  $\text{MgO}$  powder would be better provided the particle diameter is small enough. Our preliminary results with silica aerogel (low density) has yielded a precision to 9%. [Actually low-density silica aerogel is not suitable for the present purpose because it does not have the quality (i).]

Determination of the effective polarization, which depends on the details of the apparatus around the source and sample, is important in ACAR studies of spin-polarization-related phenomena such as magnetism.<sup>22</sup> In such studies the observed effects depend on the positron spin polarization as well as the electron spin polarization in the material. Because of the lack of a handy method to determine the source polarization, no one has ever done an ACAR investigation of ferromagnetic solids with a source of well-specified polarization. We suggest to prepare a suitable pressed powder tablet of the same size as the sample to be investigated and measure the source positron polarization prior to or after the main measurements.

The present method can be also used in a study of the weak interaction to measure the intrinsic longitudinal polarization of the positrons as they are emitted from nuclei. The modifications necessary for this application includes the preparation of the source with a backing made of a light material, no cover or window, and a restricted geometry for the forward beam, as employed in the lifetime based polarimeter.<sup>9,10</sup> It is also highly desirable to use the two-dimensional ACAR method, rather than one-dimensional method, in order to get high statistics with a low-intensity source.

In summary, we have demonstrated that it is actually possible by the ACAR method to separate the effect of the positron spin polarization on ortho-like-Ps and para-like-Ps formation in a magnetic field. By using this effect the spin polarization of the positron sources used in the ACAR measurements can be determined in higher accuracy than expected from the previous experiments by Page and Heinberg.<sup>1</sup>

### ACKNOWLEDGMENTS

We thank Professor K. Fujiwara for valuable discussions. We also thank Mr. S. Omi of the HOYA Corporation for providing us with the porous silica glass and ordinary silica glass made of the same raw material and for measuring the porosity of the porous glass. The experiments were performed at the Radioisotope Center of the University of Tokyo.

<sup>1</sup>L. A. Page and M. Heinberg, *Phys. Rev.* **106**, 1220 (1957); L. A. Page, *Rev. Mod. Phys.* **31**, 759 (1959).

<sup>2</sup>A. Rich, *Rev. Mod. Phys.* **53**, 127 (1981).

<sup>3</sup>S. Berko and H. N. Pendleton, *Ann. Rev. Nucl. Part. Sci.* **30**, 543 (1980).

<sup>4</sup>A. Dupasquier, in *Positron Solid State Physics*, Proceedings of the International School of Physics, "Enrico Fermi", Course 83, edited by W. Brandt and A. Dupasquier (North-Holland, Amsterdam, 1983), p. 510.

<sup>5</sup>V. L. Telegdi, cited by L. Grodzins, *Prog. Nucl. Phys.* **7**, 163 (1959).

<sup>6</sup>A. Lundby, *Prog. Elem. Part. Cosmic Ray Phys.* **5**, 1 (1960).

<sup>7</sup>L. Dick, L. Feuvrais, L. Madansky, and V. L. Telegdi, *Phys. Lett.* **3**, 326 (1963).

<sup>8</sup>A. Bisi, A. Fiorentini, E. Gatti, and L. Zappa, *Phys. Rev.* **128**, 2195 (1962).

<sup>9</sup>G. Gerber, D. Newman, A. Rich, and E. Sweetman, *Phys. Rev. D* **15**, 1189 (1977).

<sup>10</sup>M. Skalsey, T. A. Girard, D. Newman, and A. Rich, *Phys. Rev. Lett.* **49**, 708 (1982).

<sup>11</sup>A. Rich, J. Van House, D. W. Gidley, R. S. Conti, and P. W. Zitzewitz, *Appl. Phys.* **A43**, 275 (1987).

<sup>12</sup>A. Greenberger, A. P. Mills, A. Thompson, and S. Berko, *Phys. Lett.* **32A**, 72 (1970).

<sup>13</sup>R. R. Lee, E. C. von Stetten, M. Hasegawa, and S. Berko, *Phys. Rev. Lett.* **58**, 2363 (1987).

<sup>14</sup>T. Hyodo, M. Kakimoto, Y. Nagashima, and K. Fujiwara, *Phys. Rev. B* **40**, 8057 (1989).

- <sup>15</sup>S. M. Kim and J. L. Buyers, *J. Phys.* **11**, 101 (1978).  
<sup>16</sup>T. B. Chang, J. K. Deng, T. Akahane, T. Chiba, M. Kakimoto, and T. Hyodo, in *Positron Annihilation*, edited by P. C. Jain, R. M. Singru, and K. P. Gopinathan (World-Scientific, Singapore, 1985), p. 974.  
<sup>17</sup>In an ordinary least-squares fitting one fits a set of data  $\{x_i, y_i\}$  ( $i=1, \dots, n$ ) to a function  $y=f(x, a_j)$  ( $j=1, \dots, k$ ) characterized by a set of free parameters  $a_j$ . The optimum values for  $a_j$  are obtained by minimizing

$$\chi^2 = \sum_i \left[ \frac{y_i - f(x_i, a_j)}{\sigma_{y_i}} \right]^2,$$

where  $\sigma_{y_i}$  are the uncertainties in the data points  $y_i$ . We have extended this method to fit two sets of data  $\{x_i, y_i\}$  ( $i=1, \dots, n$ ) and  $\{x'_i, z_i\}$  ( $i=1, \dots, n'$ ) simultaneously to corresponding functions  $y=f(x, a_j)$  ( $j=1, \dots, k$ ) and  $z=g(x, b_j)$  ( $j=1, \dots, k'$ ) with constraints on some of the parameters  $a_j$  and  $b_j$ . The optimized values for the parameters are obtained by minimizing

$$\chi^2 = \sum_i \left[ \frac{y_i - f(x_i, a_j)}{\sigma_{y_i}} \right]^2 + \sum_i \left[ \frac{z_i - g(x'_i, b_j)}{\sigma_{z_i}} \right]^2.$$

In the first case discussed in the text  $y_i$  and  $z_i$  are the ACAR

curves for opposite field directions and the constraint is that the widths of the narrow components in the curves should be the same for the same magnitude of the fields, while in the second case  $y_i$  and  $z_i$  are  $I_n(B)+I_n(-B)$  and  $I_m(B)+I_m(-B)$  and the constraints are  $a_j=b_j$  (for all  $j$ ). In the third case  $y_i$  and  $z_i$  are  $I_m(B)$  and  $I_n(B)$  and the constraints are the same as in the second case. In all cases  $x_i=x'_i$  ( $=p_{z_i}$  or  $B_i$ ) and  $n=n'$ . See also, *Open Discussion on Experimental Techniques and Data Analysis (for Bulk Systems)*, compiled and edited by M. Eldrup, I. K. MacKenzie, B. T. A. McKee, and D. Segers, in *Positron Annihilation*, edited by L. Dorikens-Vanpraet, M. Dorikens, and D. Segers (World-Scientific, Singapore, 1989), p. 216.

- <sup>18</sup>T. Hyodo, M. Kakimoto, T. B. Chang, J. K. Deng, T. Akahane, T. Chiba, B. T. A. McKee, and A. T. Stewart, in *Positron Annihilation*, edited by L. Dorikens-Vanpraet, M. Dorikens, and D. Segers (World-Scientific, Singapore, 1989), p. 878.  
<sup>19</sup>T. Chang, M. Xu, and X. Zeng, *Phys. Lett.* **A126**, 189 (1987).  
<sup>20</sup>M. Kakimoto, T. Hyodo, T. Chiba, T. Akahane, and T. B. Chang, *J. Phys.* **B 20**, L107 (1987).  
<sup>21</sup>M. Kakimoto (unpublished).  
<sup>22</sup>See, for example, S. Berko, in *Compton Scattering*, edited by B. Williams (McGraw Hill, London, 1977), p. 273.